Solvent Effects on Self-Assembly of β-Amyloid Peptide

Chih-Lung Shen and Regina M. Murphy

Department of Chemical Engineering, University of Wisconsin, Madison, Wisconsin 53706 USA

ABSTRACT   β-amyloid peptide (Aβ) is the primary protein component of senile plaques in Alzheimer's disease patients. Synthetic Aβ spontaneously assembles into amyloid fibrils and is neurotoxic to cortical cultures. Neurotoxicity has been associated with the degree of peptide aggregation, yet the mechanism of assembly of Aβ into amyloid fibrils is poorly understood. In this work, Aβ was dissolved in several different solvents commonly used in neurotoxicity assays. In pure dimethylsulfoxide (DMSO), Aβ had no detectable β-sheet content; in 0.1% trifluoroacetate, the peptide contained one-third β-sheet; and in 35% acetonitrile/0.1% trifluoroacetate, Aβ was two-thirds β-sheet, equivalent to the fibrillar peptide in physiological buffer. Stock solutions of peptide were diluted into phosphate-buffered saline, and fibril growth was followed by static and dynamic light scattering. The growth rate was substantially faster when the peptide was predissolved in 35% acetonitrile/0.1% trifluoroacetate than in 0.1% trifluoroacetate, 10% DMSO, or 100% DMSO. Differences in growth rate were attributed to changes in the secondary structure of the peptide in the stock solvent. These results suggest that formation of an intermediate with a high β-sheet content is a controlling step in Aβ self-assembly.

INTRODUCTION

β-amyloid peptide (Aβ) is the primary protein component of senile plaques in Alzheimer's disease (AD) patients (Wong et al., 1985). It is a 39- to 43-residue proteolytic product of a membrane-associated precursor protein (Masters et al., 1985; Prelli et al., 1988; Kang et al., 1987). The peptide self-assembles into amyloid fibers, which are characterized by a cross-β-pleated sheet structure, fibril diameters of 5–10 nm, and birefringence upon staining with Congo red. Amyloid fibers are deposited extracellularly in the AD brain and are typically surrounded by degenerating cells (Merz et al., 1981).

Synthetic Aβ readily forms amyloid fibrils in vitro (Kirschner et al., 1987; Fraser et al., 1991a). A number of studies have shown that addition of synthetic Aβ to cultured cortical cells is associated with direct toxicity (see, for example, Yankner et al., 1990; Busciglio et al., 1993) or enhanced susceptibility to glutamate excitotoxicity (Koh et al., 1990; Mattson et al., 1992). Recently, transgenic mice carrying a mutant form of Aβ precursor protein have been shown to produce Aβ, develop amyloid plaques, and show some signs of neuropathology similar to AD (Games et al., 1995). The mechanism by which Aβ exerts toxic effects is unknown, although numerous hypotheses have been put forth. Differences in biological activity of Aβ solutions may be related to differences in aggregation state (Pike et al., 1991, 1993; Ueda et al., 1994), although there is some

suggestion that aggregation state alone is not sufficient to predict neurotoxicity (Busciglio et al., 1993).

Synthetic Aβ is generally difficult to dissolve directly into physiological buffers. Researchers have overcome this problem by preparing stock solutions of the peptide in a variety of solvents before dilution into culture medium or in vivo injection for assessment of biological activity. Commonly used solvents include dimethylsulfoxide (DMSO; e.g., Mattson et al., 1993), aqueous acetonitrile with trifluoroacetic acid (ACN/TFA; e.g., Abe et al., 1994; Yankner et al., 1990), and dilute aqueous TFA (e.g., Whitson et al., 1994). There is some evidence that the solvent may alter the biological activity of Aβ. Busciglio et al. (1992) measured neuronal cell death after incubation of mixed cortical cultures with synthetic Aβ. Toxicity was greatest if the peptide was first dissolved in aqueous ACN, intermediate if first dissolved in pure water, and least if first dissolved in DMSO. In contrast, Mattson et al. (1992) detected no direct toxicity of Aβ in cortical cultures but saw enhanced toxicity to glutamate in the presence of the peptide. In this case, stock solutions prepared with DMSO were 100-fold more potent than those prepared with pure water.

In this study, the influence of solvent on self-assembly of β(1–39), a synthetic peptide corresponding to the first 39 residues of Aβ, was investigated. Stock solutions of β(1–39) in 100% DMSO, 10% DMSO, 0.1% TFA, or 35% ACN/0.1% TFA were prepared. Secondary structure information was obtained for the peptide in the stock solvents using circular dichroism (CD) or Fourier transform infrared (FTIR) spectroscopy. Stock solutions were diluted into phosphate-buffered saline (PBS), and static and dynamic light scattering data were collected and analyzed to determine fibril size and growth rate. The rate of fibril growth was considerably faster when the stock solution was prepared from ACN/TFA versus DMSO. The kinetics of fibril

growth were analyzed in detail. This analysis sheds light on the mechanism of self-assembly of Aβ.

MATERIALS AND METHODS

A peptide homologous to the first 39 residues of Aβ, β(1–39), was synthesized, purified, and characterized as described previously (Shen et al., 1994). The peptide was lyophilized from aqueous ACN/TFA solution after high pressure liquid chromatography purification and stored at −70°C. Solvents used were 100% ACN (Baker, Phillipsburg, NJ); TFA, free acid form (Sigma Chemical Co., St. Louis, MO); and 99.5% ACS reagent grade DMSO (Sigma Chemical Co.).

Circular dichroism spectroscopy

β(1–39) was dissolved in 35% ACN/0.1% TFA to a final concentration of 0.2 mg/ml. The solution was filtered through a 0.45-μm Millipore (Bedford, MA) filter to remove dust and then degassed. CD spectra in the far UV (190–240 nm) range were obtained with a modified Cary model 60 spectropolarimeter (On-line Instrument Systems, Bogart, GA) as described previously (Shen et al., 1994).

Fourier transform infrared spectroscopy

Because of the strong absorbance of DMSO in the UV range, CD data could not be obtained in this solvent. Instead, FTIR spectra were collected on a Nicolet (Madison, WI) 740 FTIR instrument at a resolution of 2 cm⁻¹. β(1–39) was dissolved in pure DMSO at 5.0 mg/ml, incubated at room temperature for 1 h, and placed in CaF_2 windows with a pathlength of 150 μm. FTIR spectra were recorded and averaged from 64 scans and the contribution from DMSO was subtracted.

Gel electrophoresis

β(1–39) was radioiodinated by a modified Bolton-Hunter procedure (Good and Murphy, 1995). Unlabeled peptide was dissolved at 10 mg/ml into pure DMSO, 10% DMSO in water, 35% ACN/0.1% TFA, or 0.1% TFA and doped with 10% by volume of a 0.004 mg/ml solution of radioiodinated peptide in PBS. Aliquots were applied to a homogeneous 7.5% polyacrylamide gel (Pharmacia, Uppsala, Sweden) shortly after preparation. Gels were electrophoresed with the Pharmacia pHastgel system. X-ray film (Fuji) was exposed to unfixed gels at −70°C for 5 weeks, then developed according to the manufacturer's instructions.

Static light scattering

Stock solutions were prepared by dissolving β(1–39) (10 mg/ml) into 35% (v/v) ACN/0.1% (v/v) TFA, 0.1% (v/v) TFA, 10% (v/v) DMSO in water, or 100% DMSO. Stock solutions were incubated for 1 h at 25°C. PBS with azide (PBSA; 0.01 M K_2HPO_4/KH_2PO_4, 0.14 M NaCl, 0.02% (w/v) sodium azide) was double-filtered through a 0.22-μm filter (Millipore). Samples were prepared by diluting peptide stock solutions into PBSA and adjusting the pH to 7.4 with 0.5 N NaOH. All samples were at a final peptide concentration of 0.5 mg/ml unless otherwise specified. Each sample was filtered through a 0.45-μm filter (Millipore) directly into the light-scattering cuvette, which was temperature controlled to 25 ± 0.1°C, to initiate experiments. Static light scattering (SLS) data were collected as described previously (Shen et al., 1993, 1994). SLS data are classically analyzed by the equation:

$$\frac{Kc}{R_s(q)} = \langle M \rangle_{w,app}^{-1} \times P(q)^{-1}, \tag{1}$$

where c is the peptide concentration, $K = 4\pi^2 n^2 (dn/dc)^2/N_A\lambda_o^4$, dn/dc is the refractive index increment, N_A is Avogadro's number, λ_o is the wavelength of light in vacuo, q is the scattering vector ($= 4\pi n/\lambda_o \sin(\theta/2)$) at scattering angle θ, $\langle M \rangle_{w,app}$ is the apparent weight-average molecular weight, and $P(q)$ is the particle scattering factor. The second virial coefficient correction was ignored in Eq. 1, thus leading to the use of the subscript *app*. For convenience, the subscript will be dropped for the remainder of this report. For determination of dn/dc, solutions of peptide were made at known concentrations and the refractive index of the solution was measured using a Milton-Roy (Rochester, NY) Abbe-3L refractometer. The refractive index increments of β(1–39) in PBSA, 5% DMSO, and 10% DMSO were taken as 0.145 cm³/g, 0.180 cm³/g, and 0.180 cm³/g, respectively. For all of the samples, dn/dc was assumed independent of aggregation state.

The scattering factor $P(q)$ is a function of particle shape. Two alternative models of particle shape, wormlike chain and wormlike star, were used to fit SLS data. The wormlike chain model describes a linear chain with total contour length L_c and Kuhn statistical segment length l_k (a measure of the stiffness of the chain, equal to two times the persistence length). $P(q)$ for semiflexible wormlike chains is (Koyama, 1973)

$$P(q) = \frac{2}{L_c^2} \int_0^{L_c} (L_c - t) \times \phi(t, l_k, q) dt, \tag{2}$$

where the function $\phi(t, l_k, q)$ has been described elsewhere (Koyama, 1973; Shen et al., 1994). The continuous wormlike star model assumes that any two arms of the star is a wormlike chain, that all arms are of identical length, and that the flexibility at the branch point is the same as that of the rest of the chain. $P(q)$ for the continuous wormlike star model is a function of l_k, the contour length of one arm $L_{c,a}$, and the number of branches f (Huber and Burchard, 1989):

$$P(q) = \frac{1}{fL_{c,a}^2} \left\{ 2(2-f) \int_0^{L_{c,a}} (L_{c,a} - x)\phi dx \right.$$

$$\left. + (f-1) \int_0^{2L_{c,a}} (2L_{c,a} - x)\phi dx \right\} \tag{3}$$

Scattered intensity data were plotted as $q^2 R_s(q)/Kc$ ($= q^2\langle M \rangle_w P(q)$) versus q (Kratky plot). $\langle M \rangle_w$, l_k, L_c (or $L_{c,a}$), and, where appropriate, f were determined by nonlinear regression using the parameter estimation software program GREG (Stewart and Sorensen, 1981), with numerical integration to evaluate Eq. 2 or 3. To reduce covariances to acceptable levels, fitting was done by reparameterization to the parameter set ($\langle M \rangle_w$, L_c, $L_c l_k$) for Eq. 2 or ($\langle M \rangle_w$, $L_{c,a}$, $L_{c,a}l_k$, and $fL_{c,a}^{0.5}$) for Eq. 3. $\langle M \rangle_w$ was independently determined by extrapolation of Kc/R_s versus q^2 to $q^2 = 0$ using Eq. 1 and in all cases agreed to that determined by regression to the multiple parameter set within experimental error.

The apparent fibril diameter was calculated assuming a solid cylindrical geometry using

$$d_{app} = \left(\frac{4}{\pi} \frac{\langle M \rangle_w V_h}{N_A L_c} \right)^{0.5}, \tag{4}$$

where the estimated hydrated specific volume V_h of β(1–39) is 1.11 cm³/g (Kuntz and Kauzmann, 1974; Cohn and Edsall, 1943). For particles fit to the wormlike star model, $L_c = fL_{c,a}$ in Eq. 4.

Dynamic light scattering

Dynamic light scattering (DLS) experiments were performed as described previously (Shen et al., 1994) using the same samples as used for SLS experiments. Data were collected at 30°, 45°, 70°, 90°, and 120° scattering

angles beginning 1 h after sample preparation. Autocorrelation data were fit to a third-order cumulants expression (Koppel, 1972):

$$\ln|g^{(1)}(\tau)| = -\langle\Gamma\rangle\tau + \frac{1}{2!}\mu_2\tau^2 - \frac{1}{3!}\mu_3\tau^3 + ... \quad (5)$$

to obtain the initial decay rate $\langle\Gamma\rangle$, where $\langle\Gamma\rangle^{-1}$ can be considered a relaxation time corresponding to the time scale for motion of particles in solution. $\langle\Gamma\rangle/q^2$ was extrapolated to $q = 0$ to yield the apparent z-average mutual diffusion coefficient $D_{2,m}$. Alternatively, autocorrelation data were fit to a biexponential form:

$$g^{(1)}(\tau) = A_f \exp(-\Gamma_f\tau) + A_s \exp(-\Gamma_s\tau) , \quad (6)$$

where $\Gamma_f = D_f q^2$ and $\Gamma_s = D_s q^2$ correspond to fast and slow diffusive modes with amplitude A_f and A_s and diffusivities D_f and D_s, respectively.

The theoretical translational diffusion coefficient $D_{Y\text{-}F}$ for wormlike chains was calculated from L_c and l_k using the equations of Yamakawa and Fujii (1973). For wormlike stars, $D_{Y\text{-}F}$ was calculated from the same equations, assuming that $L_c = fL_{c,a}$ (Burchard et al., 1980).

Thioflavin T fluorescence spectroscopy

Thioflavin T (ThT; Sigma Chemical Co.) was dissolved at 100 μM in PBSA. The peptide was dissolved at 10 mg/ml in each of the stock solvents, incubated for 1 h at 25°C, then diluted 20-fold into PBSA. At various time intervals after dilution, 40 μl of peptide solution and 40 μl of ThT stock solution were mixed with 920 μl of PBSA. The mixture was briefly vortexed before obtaining fluorescence measurements. Fluorescence emission spectra were taken from 460 nm to 500 nm at an excitation

wavelength of 450 nm with a Model M-3 Alphascan (Photon Technology International, South Brunswick, NJ) spectrofluorimeter and a 1 × 0.4 cm² cuvette at a temperature of 25 ± 0.1°C. Triplicate measurements were performed for each sample. A maximum at 482 nm was indicative of the presence of amyloid (LeVine, 1993). Fluorescence intensity for diluted ThT in the absence of peptide was determined and subtracted from sample intensities.

RESULTS

Characterization of peptide in stock solutions

CD spectra for $\beta(1-39)$ in 0.1% TFA and in 0.01 M phosphate, pH 7.4, were reported previously (Shen et al., 1994). Quantitative analysis of the CD spectra indicated that the peptide retained some conformation in 0.1% TFA, with approximately one-fourth β-turn, one-third β-sheet, and the remainder disordered. In 35% ACN/0.1% TFA, CD spectra of the peptide was similar to the peptide in phosphate buffer (Fig. 1 A). Fitting of the spectra yielded an estimate of the peptide conformation as approximately two-thirds β-sheet and one-third disordered in either ACN/TFA or phosphate buffer. FTIR spectra for the peptide in 100% DMSO had no detectable peak at 1640–1620 cm^{-1}, indicating that the peptide has no β-sheet content in this solvent (Fig. 1 B). FTIR cannot be used to discriminate readily between α-helical and random coil conformations; NMR studies indicated that the peptide $\beta(1-28)$ is partially α-helical and partially random coil in DMSO (Sorimachi and Craik, 1994).

Stock solutions of $\beta(1-39)$ migrated with the dye front when subjected to native gel electrophoresis on a 7.5% polyacrylamide gel (data not shown). Light scattering from samples of 0.5 mg/ml $\beta(1-39)$ in 100% DMSO, 0.1% TFA, or ACN/TFA was too weak to be detectable above noise. (Analysis of samples at the stock concentrations, 10 mg/ml, was not done because of the prohibitively large quantity of peptide required.) Scattering was sufficiently strong to be measured for 0.5 mg/ml $\beta(1-39)$ in 10% DMSO. Intensity data for this solution were plotted as $q^2 R_s/Kc$ ($= q^2\langle M\rangle_w P(q)$) versus q (Fig. 2) and fit using $P(q)$ of a
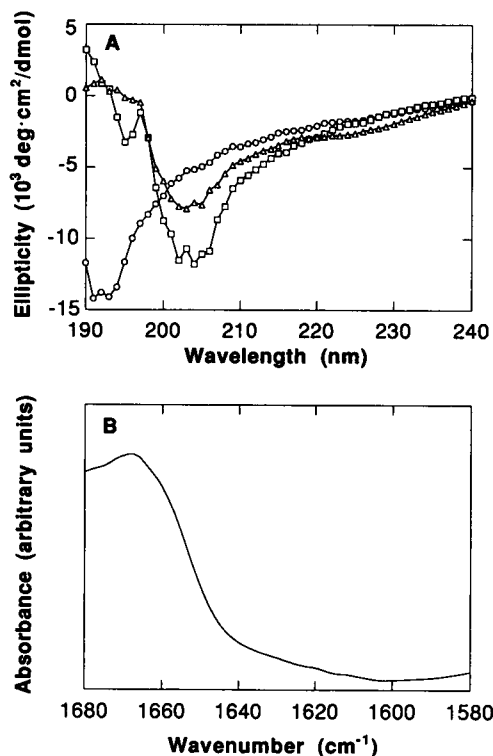

FIGURE 1   Secondary structure of $\beta(1-39)$ as a function of solvent. (A) CD spectra of $\beta(1-39)$ at 0.2 mg/ml in 35% ACN/0.1% TFA ($\triangle$), 0.1% TFA ($\bigcirc$), or phosphate buffer ($\square$). (B) FTIR spectra of $\beta(1-39)$ at 5 mg/ml in 100% DMSO. The broad peak near 1665 cm^{-1} is a result of residual TFA from the lyophilized peptide and α-helical or random coil conformation.
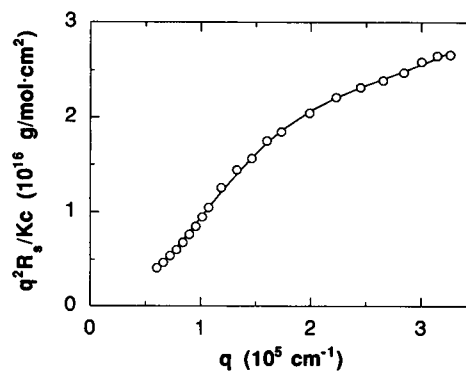

FIGURE 2   Kratky plot of 0.5 mg/ml $\beta(1-39)$ in 10% DMSO. The solid line represents the nonlinear least-squares fit of the data using the wormlike chain model (Eq. 2).

wormlike chain (Eq. 2). Particles had an average molecular mass $\langle M \rangle_w$ of $1.2 \pm 0.1 \times 10^6$, an average contour length L_c of 360 ± 30 nm, and an average Kuhn statistical length l_k of 230 ± 10 nm. $\langle M \rangle_w$ and $D_{z,m}$ $(2.3 \pm 0.3 \times 10^{-8}$ cm^2/sec) did not change significantly over a 48-h measurement period. The apparent fibril diameter was calculated from Eq. 4 as 2.8 nm. These fibrillar aggregates were amyloid as evidenced by positive staining with Congo red and ThT (data not shown). Electron microscopic examination confirmed the presence of fibrils with some curvature in this solvent mixture (data not shown).

Effect of stock solvent on aggregation rate

The kinetics of aggregation were determined by DLS. Data collection was stopped when signal quality decreased, which was concomitant with the appearance of visible precipitates. $D_{z,m}^{-1}$, which is proportional to the effective hydrodynamic radius from the Stokes-Einstein equation, was calculated from a cumulants fit to the data (Eq. 5) and plotted in Fig. 3 as a function of time and initial stock solvent. $D_{z,m}^{-1}$ for the sample made from the ACN/TFA stock solution increased rapidly. In sharp contrast, $D_{z,m}^{-1}$ for samples prepared by dilution of TFA or 10% DMSO stocks increased at intermediate rates, and $D_{z,m}^{-1}$ for the sample prepared from dilution of 100% DMSO stock solution increased slowly. Precipitates were observed both visually and by a decay in signal quality approximately 12 h or 4, 5, or 9 days after dilution from ACN/TFA, 10% DMSO, TFA, or 100% DMSO, respectively, into PBSA.

ThT fluorescence as a function of stock solvent was determined (Fig. 4). Initially, the sample prepared from DMSO stock solvent had a lower ThT fluorescence intensity compared with 0.1% TFA or 10% DMSO stock solvents, paralleling results of the DLS measurements. The rate of increase of fluorescence intensity was slow for the first 3–4 days, then increased sharply after 4–8 days. After 8 days, fluorescence intensity for all three samples was similar. The jump in fluorescence intensity correlated approx-
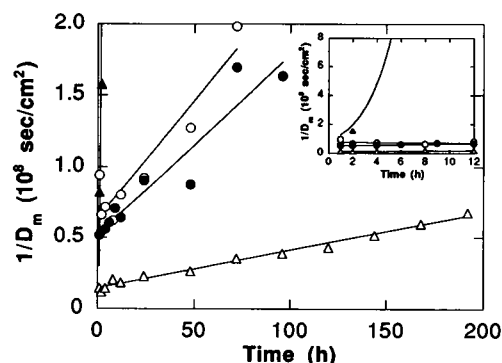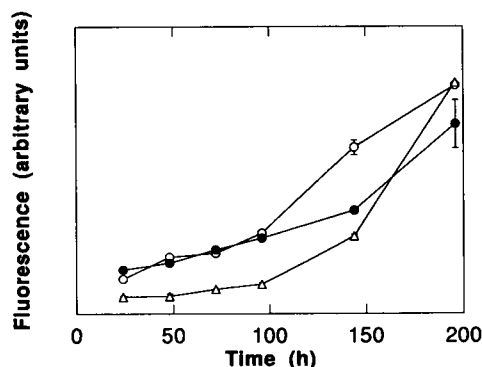

FIGURE 4 ThT fluorescence intensity as a function of initial solvent. Fluorescence intensity was measured at 482 nm with excitation at 450 nm for 0.5 mg/ml in PBSA, with stock solution prepared at 10 mg/ml peptide in 10% DMSO (O), 0.1% TFA (●), or 100% DMSO (△).

imately with the appearance of visible precipitates in light scattering measurements.

Solvent effects on fibril dimensions

For samples prepared in the stock solvents 100% DMSO, 0.1% TFA, 10% DMSO, or ACN/TFA, SLS data were collected 12 h after dilution of the peptide stock solution into PBSA. For the sample made from ACN/TFA stock solution, large fluctuations in the average scattered intensity resulting from incipient precipitation precluded collection of SLS data.

Intensity data were plotted as $q^2 R_s/Kc$ $(= q^2 \langle M \rangle_w P(q))$ versus q for samples prepared from stock solutions of 100% DMSO, 0.1% TFA, or 10% DMSO diluted 20-fold into PBSA (Fig. 5). Comparison of the shape of each curve indicates that particle morphologies differ among the three samples. The shape of the curve for the sample prepared from 100% DMSO stock solution (Fig. 5 A) is typical for a linear, nonbranching, semiflexible chain (Schmidt et al., 1985). In contrast, the appearance of a bump at intermediate values of q indicates that fibrils of β(1–39) may contain some branched structures (Burchard, 1977; Burchard and Muller, 1980) when prepared from stock solutions of 0.1% TFA (Fig. 5 B) or 10% DMSO (Fig. 5 C).

To fit the particle structure factor $P(q)$ to the data, assumptions regarding particle morphologies were needed. Based on electron micrographs (not shown), the particles were assumed to be semiflexible fibrils and therefore could be modeled as wormlike chains using Eq. 2. Where this particle morphology inadequately represented the experimental particle structure data, the wormlike star model (Huber and Burchard, 1989) was used. In Fig. 5, nonlinear regression fits to the wormlike chain and/or the wormlike star models are shown. For the sample prepared from 100% DMSO, the simpler wormlike chain model accurately represented the angular dependence of the scattered intensity. For the sample prepared from 0.1% TFA, although a fairly good fit to the wormlike chain model was obtained, the

FIGURE 3 Aggregation rate as a function of initial solvent. Inverse apparent mutual diffusion coefficient $D_{z,m}^{-1}$ for β(1–39) at 0.5 mg/ml in PBSA, with stock solution prepared at 10 mg/ml peptide in 35% ACN/0.1% TFA (▲), 10% DMSO (O), 0.1% TFA (●), or 100% DMSO (△).
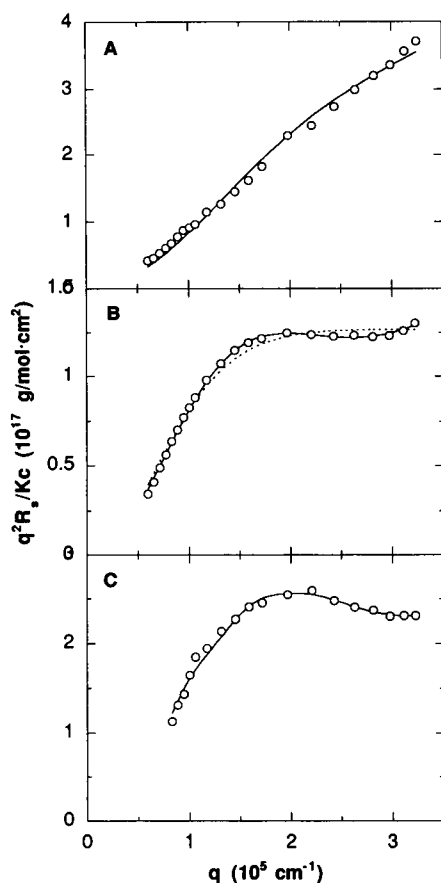
FIGURE 5   Representative Kratky plots for SLS data taken 12 h after sample dilution. All samples were prepared by 20-fold dilution of 10 mg/ml stock into PBSA. (A) 100% DMSO stock solution. The solid line represents the fit to the data using the wormlike chain model (Eq. 2). (B) 0.1% TFA stock solution. The solid line represents the fit to the data using the wormlike star model (Eq. 3) and the dotted line represents the fit to the data using the wormlike chain model. (C) 10% DMSO stock solution. The solid line represents the fit to the data using the wormlike star model.

additional parameter in the wormlike star model produced a statistically improved fit. For the sample prepared from 10% DMSO, convergence to the wormlike chain model was not obtained, but fitting to the wormlike star model was good.

Results from fitting the data in Fig. 5 are summarized in Table 1. $\langle M \rangle_w$, $L_{c,a}$, and L_c increased in the order 100% DMSO < 0.1% TFA < 10% DMSO. The degree of branching also depended on initial conditions; the sample made from 100% DMSO was unbranched, whereas samples made from 10% DMSO and 0.1% TFA showed a low degree of branching. Fibril stiffness in samples made from 10% DMSO and 0.1% TFA was identical. l_k could not be determined by regression for the sample made from 100% DMSO, indicating that the Kuhn length of these fibrils approaches the contour length of the fibril. The apparent fibril diameter d_{app} was calculated from $\langle M \rangle_w / L_c$, where $L_c = f L_{c,a}$, using Eq 4. The data are included in Table 1. d_{app} increases for samples prepared from different stock solutions in the order 100% DMSO < 0.1% TFA < 10% DMSO.

TABLE 1   Effect of stock solvent on aggregate size and morphology

	Stock solvent		
	100% DMSO	0.1% TFA	10% DMSO
$\langle M \rangle_w$ (10^6 Da)	1.14 ± 0.07	12.1 ± 0.3	25 ± 1
$L_{c,a}$ (nm)	230 ± 20*	290 ± 40	280 ± 40
l_k (nm)	ND[‡]	150 ± 10	140 ± 20
f	NA[§]	3.2 ± 0.4	3.8 ± 0.4
L_c ($=f L_{c,a}$) (nm)	230 ± 20	900 ± 200	1100 ± 300
d_{app} (nm)	3.4 ± 0.1	5.6 ± 0.2	7.5 ± 0.3

β(1–39) was dissolved at 10 mg/ml in the stock solvent, then diluted into PBSA to 0.5 mg/ml. Results are from SLS data taken 12 h after sample dilution.
* L_c, not $L_{c,a}$.
[‡] Not determined.
[§] Not applicable in wormlike chain model.

DLS data taken 12 h after sample dilution were analyzed using Eq. 6. The existence of well separated fast and slow diffusive modes was apparent at all angles for the ACN/TFA, 10% DMSO, and TFA samples. No slow mode was reliably detected for the DMSO sample. Results from fitting the DLS data are summarized in Table 2 and compared with theoretical calculations for the translational diffusion coefficient $D_{Y\text{-}F}$. These calculations show reasonable agreement between the measured D_f and the theoretical $D_{Y\text{-}F}$ for individual fibrils. Thus, D_f can be ascribed to diffusion of individual fibrils. Interpretation of slow diffusive modes is still controversial. Given the strong dependence of D_s on scattering angle and time for our samples, D_s may be attributed to diffusion of large aggregates of fibrils (Seery et al., 1992; Drogemeier et al., 1994).

By using DLS data for this sample, D_f and D_s for the sample diluted from ACN/TFA were determined. Assuming $l_k = 150$ nm and $d = 5$ nm, and by using the Yamakawa-Fujii relationships, L_c for this sample was estimated from D_f. DLS data taken 1 h after sample dilution for all four

TABLE 2   Effect of stock solvent on hydrodynamic properties of fibril aggregates

	Stock solvent			
	100% DMSO	0.1% TFA	10% DMSO	ACN/TFA
1 h				
D_f (10^{-8} cm²/s)	13 ± 1	7 ± 2	4 ± 1	2.4 ± 0.4
D_s (10^{-8} cm²/s)	0.7 ± 0.4	1.7 ± 0.2	1.1 ± 0.2	0.81 ± 0.01
L_c* (nm)	150	300	700	1500
12 h				
D_f (10^{-8} cm²/s)	5.6 ± 0.7	4 ± 1	3 ± 1	0.33 ± 0.04
D_s (10^{-8} cm²/s)	0.0 ± 0.4	1.0 ± 0.2	0.99 ± 0.07	0.03 ± 0.01
$D_{Y\text{-}F}$ (10^{-8} cm²/s)	8.7	3.3	3.1	
L_c* (nm)	450	700	1100	>10^4

β(1–39) was dissolved at 10 mg/ml in the stock solvent, then diluted into PBSA to 0.5 mg/ml. Results are from DLS data taken 1 h and 12 h after sample dilution.
* Estimated from D_f using the Yamakawa-Fujii (1973) equations and assuming $l_k = 150$ nm and $d = 5$ nm.

samples were similarly analyzed and used to estimate L_c. Results from these calculations are included in Table 2. These results show that, at 1 h after sample dilution, long fibrils have already formed and, at both 1 h and 12 h after sample dilution, fibril length increases in the order 100% DMSO < 0.1% TFA < 10% DMSO < ACN/TFA.

SLS data were collected for samples over time and analyzed for fibril characteristics (Figs. 6 and 7). $\langle M \rangle_w$ and L_c both increased with time for all three samples. There was no evidence of branching at any time in the 100% DMSO sample. In contrast, samples prepared from 10% DMSO and 0.1% TFA both showed a low degree of branching, with the degree of branching increasing slowly with time. For all three samples, l_k remained constant or decreased slightly with time, within experimental error. The Kuhn length decreased with increasing L_c, suggesting that fibril stiffness may be a weak inverse function of contour length.

For the sample prepared from 100% DMSO, the increase in the average molecular weight $\langle M \rangle_w$ correlated with an

FIGURE 7 Fibril morphology as a function of time and solvent. See Fig. 6 legend for details. (A) Kuhn statistical segment length l_k. (B) Number of branches f ($f = 2$ for an unbranched chain). (C) The apparent fibril diameter d_{app}, calculated using Eq. 4.

increase in the contour length L_c of the fibril. For the samples prepared from 0.1% TFA or 10% DMSO stock solutions, the increase in $\langle M \rangle_w$ was accompanied by both an increase in degree of branching f and an increase in the contour length $L_{c,a}$. The apparent diameter d_{app}, calculated by using Eq. 4, was constant or increased only very slightly with time for all three samples.

We attempted to determine the polydispersity of the samples by incorporating the Schulz-Zimm distribution into the particle scattering factor (Gamini and Mandel, 1994). Fitting of the light scattering data to this model resulted in determination that the fibril size distribution was essentially monodisperse.
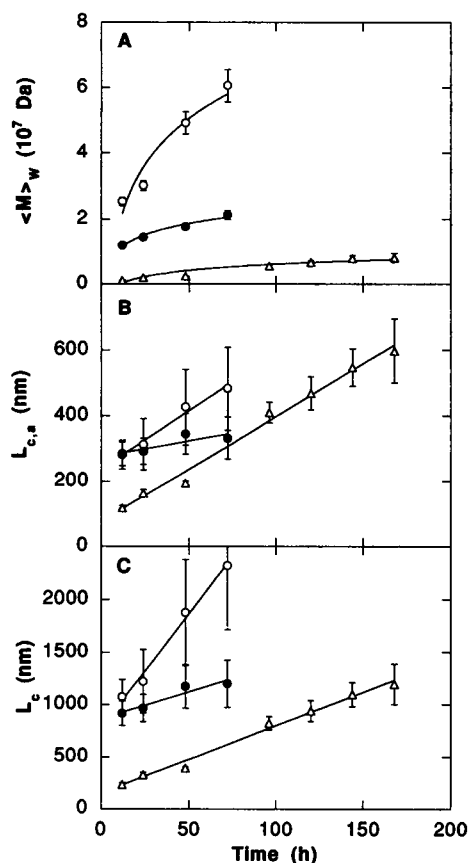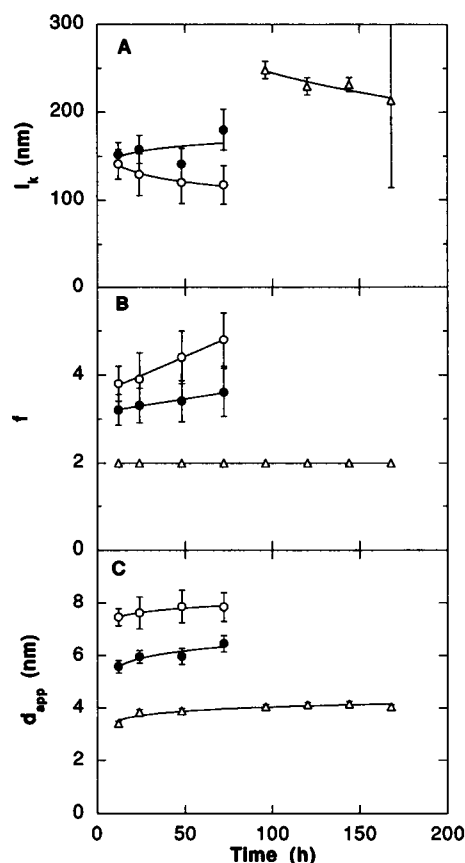

FIGURE 6 Fibril size as a function of time and initial solvent. All samples were prepared by 20-fold dilution of stock solutions at 10 mg/ml into PBSA. Kratky plots were fit to the wormlike chain model (100% DMSO stock solution, △) or the wormlike star model (0.1% TFA, ●; and 10% DMSO stock solutions, ○). (A) Weight-average molecular weight, $\langle M \rangle_w$. (B) Contour length of an arm, $L_{c,a}$. For the sample prepared from 100% DMSO, $L_{c,a}$ was calculated from the fitted value of L_c by dividing by 2, the number of "branches" in an unbranched chain. (C) Total contour length, L_c. For samples prepared from 0.1% TFA or 10% DMSO, $L_c = fL_{c,a}$.

Effect of peptide concentration on fibril growth from 0.1% TFA

Samples were prepared by dissolving 10 mg/ml β(1–39) in 0.1% TFA, incubating for 1 h, and then diluting into PBSA to a final concentration of 0.1–1 mg/ml. SLS data were collected for samples at final peptide concentrations of 0.3, 0.5, and 1.0 mg/ml and fit with the wormlike star model (Eq. 3). Results from data taken 12 h after dilution are

summarized in Table 3. $\langle M \rangle_w$, l_k, and d_{app} did not change significantly with concentration. L_c, $L_{c,a}$, and f increased with decreasing concentration, but the differences were not statistically significant. Results from analysis of DLS data taken 12 h after sample dilution are included in Table 3. D_{Y-F} was calculated as described previously and compared with D_f. These data show a decrease in fibril diffusivity (increase in fibril length) with decreasing concentration. At lower peptide concentrations (0.1–0.2 mg/ml), signal intensity was sufficient to collect DLS but not SLS data. D_f and D_s were determined from DLS data for five concentrations (0.1–1 mg/ml) taken 1 h after sample dilution (Table 4). L_c was calculated from D_f as described previously. Again, there is an indication that the fibril length is greater (D_f is smaller) at the lower concentrations.

Variability in samples prepared from DMSO stock solution

Light scattering data for samples prepared from stock solutions of 0.1% TFA or ACN/TFA were reproducible (data not shown). In contrast, samples prepared from 100% DMSO stock solution and diluted to a final peptide concentration of 0.5 mg/ml exhibited two types of behavior. Results from cumulants analysis of DLS data for four independent runs are shown in Fig. 8. The increase in $D_{z,m}^{-1}$ of the peptide solution prepared from this solvent appeared to follow one of two pathways: slow growth, as shown previously in Fig. 3, or rapid growth, intermediate between that for 0.1% TFA and ACN/TFA stock solutions. For the samples that grew rapidly, visible precipitates after ~12 h were observed. For one rapidly growing sample, SLS data were collected at 12 h and analyzed. $\langle M \rangle_w$ was $1.1 \pm 0.1 \times 10^7$, or approximately 10-fold greater than that obtained for two other samples prepared from DMSO stock solution and analyzed. These fibrils were extremely long (2200 ± 300 nm) but with no evidence of branching. d_{app} was 3.4 nm, similar to the slowly growing sample.

Results from cumulants analysis of DLS data for two samples diluted from 100% DMSO to a final peptide concentration of 1 mg/ml are included in Fig. 8 for comparison.

TABLE 3   Effect of concentration on aggregate size and morphology

	Concentration (mg/ml)		
	0.3	0.5	1.0
$\langle M \rangle_w$ (10^6 Da)	15.6 ± 1.1	12.1 ± 0.3	12.3 ± 0.4
$L_{c,a}$ (nm)	310 ± 70	290 ± 40	230 ± 50
l_k (nm)	160 ± 30	150 ± 10	180 ± 20
f	3.5 ± 0.7	3.2 ± 0.4	3.0 ± 0.6
L_c (=$fL_{c,a}$) (nm)	1100 ± 500	900 ± 200	700 ± 300
d_{app} (nm)	5.8 ± 0.4	5.6 ± 0.2	6.5 ± 0.4
D_f (10^{-8} cm^2/s)	2.3 ± 0.2	4 ± 1	4.4 ± 0.7
D_s (10^{-8} cm^2/s)	0.57 ± 0.05	1.0 ± 0.2	1.1 ± 0.1
D_{Y-F} (10^{-8} cm^2/s)	2.8	3.3	3.7

β(1–39) was dissolved at 10 mg/ml in 0.1% TFA, then diluted into PBSA. Results are from data taken 12 h after sample dilution.

Analysis of SLS data at 12 h after sample dilution gave $\langle M \rangle_w = 9 \pm 0.7 \times 10^6$, $L_c = 720 \pm 40$ nm, $l_k = 170 \pm 10$ nm, and $d_{app} = 5.4 \pm 0.2$ nm, with no branching.

Effect of residual solvent

In preparing the sample from stock solutions, some residual solvent is present in the final sample. To determine whether the residual solvent influenced peptide assembly, samples were prepared from 0.1% TFA stock solution, diluted into PBSA containing 5% (v/v; 1.2 mol%) DMSO or 1.75% (v/v; 0.95 mol%) ACN, and analyzed by dynamic and static light scattering. D_f, D_s, and $\langle M \rangle_w$ were essentially indistinguishable from the peptide prepared from 0.1% TFA stock solution and diluted into PBSA (Fig. 9). Adjusting the concentration of TFA in the final solution in the range 0.001–0.005% had no effect on DLS results (data not shown). These data show that the residual solvent does not have a significant effect on fibril growth.

DISCUSSION

Neurotoxicity of Aβ has been demonstrated in multiple studies (e.g., Yankner et al., 1990; Loo et al., 1993; Busciglio et al., 1993; Games et al., 1995). Increasing degrees of peptide aggregation may correlate with increasing levels of neurotoxicity (Pike et al., 1991, 1993; Ueda et al., 1994). In most studies of Aβ neurotoxicity, however, aggregation has not been measured at all or has been loosely defined as material that precipitates or that sediments with centrifugation. To interpret neurotoxicity assays, to evaluate the role of aggregation in toxicity, and to develop therapeutic approaches for intervention in Aβ-mediated neurotoxicity, a more thorough knowledge of the mechanism of self-assembly of Aβ is needed.

The purpose of this investigation was to determine the effect of predissolution of Aβ in various stock solvents on Aβ self-assembly. Predissolution in stock solvents is commonly practiced to overcome the limited solubility of Aβ in physiological buffers used in neurotoxicity assays. Our results clearly demonstrate that the rate of increase in fibril length or $\langle M \rangle_w$ in PBS is a strong function of the stock solvent and is correlated to the secondary structure of the peptide in the stock solvent. Consideration of the role of solvent in determining the aggregation rate and extent yields insight into the pathway and rate-limiting steps of Aβ self-assembly.

β(1–39) contains the same degree of β-sheet in ACN/ TFA as in phosphate buffer at neutral pH. In contrast, the peptide has no β-sheet content when dissolved in 100% DMSO. ACN and DMSO are both polar aprotic solvents and are both capable of acting as hydrogen bond acceptors. However, their properties differ in significant ways. In particular, ACN forms hydrogen bonds with water that are weaker than water-water hydrogen bonds (Marcus and Migron, 1991; Kovacs and Laaksonen, 1991), whereas DMSO

TABLE 4   Effect of concentration on hydrodynamic properties of fibrils

	Concentration (mg/ml)				
	0.1	0.2	0.3	0.5	1.0
D_f (10^{-8} cm^2/s)	5 ± 1	5.4 ± 0.7	8 ± 2	7 ± 2	7 ± 1
D_s (10^{-8} cm^2/s)	1.3 ± 0.3	1.0 ± 0.1	1.4 ± 0.3	1.7 ± 0.2	1.3 ± 0.1
L_c^* (nm)	500	450	250	300	300

β(1–39) was dissolved at 10 mg/ml in 0.1% TFA, then diluted into PBSA. Results are from DLS data taken 1 h after sample dilution.

* Estimated from D_f using the Yamakawa-Fujii (1973) equations and assuming $l_k = 150$ nm and $d = 5$ nm.

forms long lasting hydrogen bonds with water that are stronger than water-water hydrogen bonds (Migron and Marcus, 1991; Luzar and Chandler, 1993). ACN in aqueous solutions disrupts protein tertiary structure by solubilizing hydrophobic regions, as a result of the decrease in solvent polarity (Mant and Hodges, 1992). Addition of ACN to water also lowers the dielectric constant, so that electrostatic repulsive interactions present at low pH are enhanced. However, ACN can actually increase the stability of secondary structures, probably because of a change in the relative strength of the peptide-peptide hydrogen bond vis-a-vis the peptide-water hydrogen bond (Mant and Hodges, 1992). In sharp contrast, DMSO competes effectively with peptide carbonyl groups for hydrogen bonding to peptide amine groups, thus destabilizing secondary structures. Pure DMSO can lead to a complete loss of secondary structure in proteins with high β-sheet content (Jackson and Mantsch, 1991). Thus, the two organic solvents have opposing effects on Aβ secondary structure. In pure DMSO, Aβ appears to be monomeric (Snyder et al., 1994) and lacks any β-sheet character (this work); in ACN/TFA, Aβ is present as a multimer (Snyder et al., 1994) with considerable β-sheet content (this work), but extensive self-assembly is inhibited, probably primarily by inhibition of hydrophobically driven association.

In dilute TFA (pH ~2), protonation of basic side chains results in the loss of any ion pairing interactions that may stabilize fibrils (Kirschner et al., 1987; Fraser et al., 1991b, 1992, 1994) and leads to electrostatic repulsion, particularly
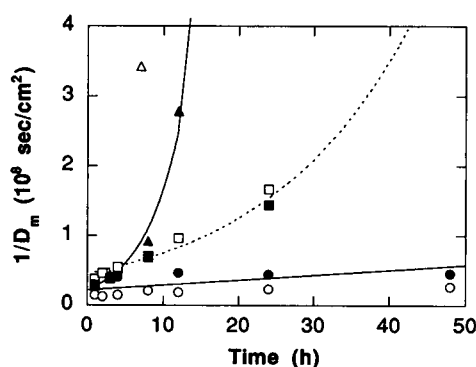

FIGURE 8   Variability in aggregation rate for samples prepared from 100% DMSO stock solutions. Four representative runs are shown in which the final peptide concentration was 0.5 mg/ml (▲, △, ●, ○). Two runs are shown in which the final peptide concentration was 1 mg/ml (■ or □).

between N-terminal segments of this amphiphilic peptide. These forces result in the retention of some β-turn and β-sheet structure, although the structure is clearly different from that of the peptide at neutral pH. CD measurements do not distinguish between mixtures of conformers or mixed conformations in a single peptide molecule. We have previously reported that β(1–39) in 0.1% TFA elutes as a single peak on a size exclusion column with a molecular weight intermediate between monomer and dimer (Shen et al., 1994). Thus, in this solvent, β(1–39) may exist as a monomer or dimer with partial β-sheet character or as a mixture of disordered monomer and β-sheet dimer.

The secondary structure of Aβ in 10% DMSO was not directly measured. However, from light scattering and ThT fluorescence assays, it is clear that this solvent mixture does not prevent amyloid fibril formation. This low concentration of DMSO is unlikely to be sufficient to disrupt secondary structure (Jackson and Mantsch, 1991). Unlike the other samples diluted into PBSA, fibrils in 10% DMSO reach what appears to be a stable size. This could be a result of the combined effect of DMSO-mediated interference with hydrogen bonding in extended β-sheets, reduced importance of hydrophobic interactions because of the absence of salt, and pH effects (as the solution was not buffered).

Upon dilution into PBSA, all peptide solutions aggregated into amyloid fibrils. Increases in size, as quantified by $D_{z,m}^{-1}$, $\langle M \rangle_w$, or L_c, continued unabated for hours to days, until the onset of precipitation. The rate of increase in size depended strongly on the stock solvent. The amyloid nature of the fibrils was indicated by ThT fluorescence. Fluorescence intensity for the peptide sample prepared from 100% DMSO was lower than for samples prepared from 10% DMSO or 0.1% TFA for the first several days. Taken together, these data indicate that the degree of β-sheet structure of the peptide in the initial solvent, the ThT fluorescence intensity, and the fibril growth rate are all generally lowest for solutions prepared from 100% DMSO, intermediate for solutions prepared from 0.1% TFA or 10% DMSO, and greatest for solutions prepared from ACN/TFA.

The correlation between β-sheet content in the stock solvent and fibril growth rate after dilution suggests that the structure of the peptide in the stock solvent is "remembered" upon dilution. Several workers have presented evidence that folding of Aβ into a β-sheet-containing structure is intermolecular (Barrow et al., 1992) and that dimers are formed (Hilbich et al., 1991; Sweeney et al., 1993). These
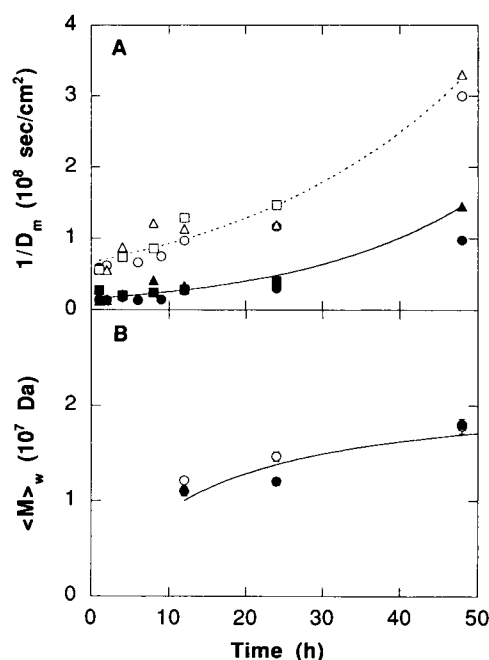
FIGURE 9 Effect of residual solvent on aggregation rate. Samples were prepared from 10 mg/ml stock solution in 0.1% TFA and diluted 20-fold into PBSA, PBSA to which 5% (v/v) DMSO was added or PBSA to which 1.75% (v/v) ACN was added. (A) D_f (solid symbols) and D_s (open symbols) when stock solution was diluted into PBSA (● or ○), PBSA plus DMSO (▲ or △), or PBSA plus ACN (■ or □). (B) $\langle M \rangle_w$ when stock solution was diluted into PBSA (○) or PBSA plus DMSO (●).

data can be explained by postulating that the first step in the self-assembly of Aβ is formation of a β-sheet dimer from monomers. The equilibrium constant for this reaction depends strongly on the solvent. Our work suggests that, in PBSA, both the forward reaction (conversion of monomer into β-sheet dimer) and the reverse reaction (dissociation of the dimer and loss of β-sheet content) must be slow relative to the rate of further association of the dimer into higher order aggregates. Otherwise, the peptide structure in the initial solvent would be irrelevant, and the monomer in DMSO and the β-sheet multimer in ACN/TFA would both rapidly revert to the same starting point before continued self-assembly, in contrast to what we observe.

Characterization of fibril dimensions in solution was carried out with SLS by selecting appropriate particle structure factors. For some samples, the wormlike chain model provided a good representation of $P(q)$. The continuous wormlike star model was chosen to represent light scattering data where a bump in the Kratky plot showed that the wormlike chain model was insufficient. This model requires that the chain length of each arm is identical, which is clearly not realistic. Still, it is the simplest model that includes both branching and chain stiffness and is a useful, albeit somewhat artificial, construct that accomodates inclusion of the concept of branching. The degree of branching is generally quite low. We envision branching as an indication that fibrils become partially entangled if the number density and length becomes sufficiently large.

The apparent fibril diameter d_{app}, as calculated from the mass linear density $\langle M \rangle_w/L_c$, varied from 3.4 to 7.5 nm, depending on the stock solvent. Fibrils of β(1–38) and β(1–40) were reported to have diameters of 7–9 nm from electron microscopy studies (Fraser et al., 1991a). Direct comparison of these values is uncertain because a solid cylinder and tube with identical diameters on electron micrographs would have considerably different mass linear densities. Several possibilities must be considered to explain the variability in d_{app} with solvent. First, when starting from different secondary structures and degrees of oligomerization, it is possible that the self-assembly pathway is affected. For example, it has been hypothesized that Aβ fibrils are cylindrical micelles with the hydrophobic terminal regions of the peptides clustered at the center of the fibril (Soreghan et al., 1994). If starting conditions affected the number of peptide monomers incorporated into each cross-sectional ring of the micelle, then the fibril diameter would be altered. Or, the degree of lateral alignment of thin filaments into fibrils could depend on the stock solvent. Alternatively, d_{app} may reflect the weight fraction of peptide in amyloid fibril form. L_c is indicative of fibril length only, whereas $\langle M \rangle_w$ is a weight-averaged molecular weight that incorporates contributions from smaller molecular weight species, if present, as well as fibrils. Under this assumption, the weight fraction of peptide incorporated into fibrils increases in the order 100% DMSO < 0.1% TFA < 10% DMSO. This order is reasonably consistent with ThT fluorescence data and with the degree of branching. An increasing weight fraction of peptide in fibrillar form should lead to an increased number and length of fibrils, which in turn would cause an increase in fibril entanglement as detected by increasing degrees of branching. The fact that d_{app} is nearly constant with time argues against a significant role of lateral alignment as a major reason for the variation in d_{app} with stock solvent. d_{app} of fibrils in 10% DMSO stock solution was very small (2.8 nm), yet electron micrographs of these fibrils did not reveal any obvious differences in fibril diameter from samples diluted into PBSA (not shown). This observation, coupled with data showing that monomers, dimers, and/or other small oligomers are detected in amyloid fibril-containing solutions (Hilbich et al., 1991; Shen et al., 1993; Snyder et al., 1994; Soreghan et al., 1994), supports, but does not prove, the assignment of differences in d_{app} to differences in weight fraction peptide in fibrillar form.

If d_{app} scales with the weight fraction of peptide in fibrillar form, then an increase in $\langle M \rangle_w/L_c$ with time would indicate that more nonfibrillar peptide was being converted to fibrillar form. However, d_{app} (or $\langle M \rangle_w/L_c$) increased only slightly with time. Under this assumption, then, the growth in L_c and $\langle M \rangle_w$ for times greater than 12 h would be due primarily to the continuing end-to-end association of shorter fibrils into longer fibrils and, to a much lesser extent, to the conversion of monomers or multimers into fibrils. Thus, the increase in size that we observe over time would be associated with an increase in fibril length but a decrease in

fibril number density to maintain a nearly constant weight fraction of peptide in fibril form. ThT results show only a very slight increase in fluorescence intensity for the first several days. This shows that fluorescence intensity is not sensitive to changes in the average size of the fibrils but may be related to the total fibril mass of the solution. The increase in fluorescence intensity after several days occurred on a time frame similar to the visual observation of precipitates. If the peptide solution was agitated, both faster formation of visible precipitates and a dramatic increase in fluorescence intensity were observed (data not shown). Thus, it is likely that ThT fluorescence intensity is also a strong function of degree of solubilization.

For samples diluted from 0.1% TFA to different final peptide concentrations, fibril length appeared to increase with decreasing concentration. One possible explanation for this phenomenon follows. The initial condition in the stock solvent may be the primary determinant of the β-sheet content in the diluted sample, as described above. Thus, decreasing the final peptide concentration would decrease the absolute concentration of β-sheet dimers but not the fraction of peptide in the β-sheet conformation. If formation of a higher-order multimer by association of several β-sheet dimers is needed to initiate fibril formation, this process would be highly concentration dependent because of the high reaction order. Subsequent fibril elongation could require addition of dimers to the multimer or growing fibril or end-to-end association of existing fibrils into longer fibrils, both second-order processes. As the concentration decreased, fibril elongation would be increasingly favored over fibril initiation. Furthermore, if fibril elongation processes are diffusion limited, dimer addition would be faster than end-to-end fibril-fibril association. The net effect would be a decrease in the number of fibrils but an increase in fibril length as peptide concentration decreased. This mechanism could also explain the variability in fibril growth rate for samples prepared from DMSO stock solutions. d_{app} was identical for both rapidly and slowly growing peptide from 100% DMSO stock solution, so, using the arguments above, the weight fraction of peptide in fibrillar form was also identical. The rapidly growing sample could be one in which there are few, very long fibrils, and the slowly growing sample could be one in which there are more numerous, but shorter, fibrils. Stock solutions of 100% DMSO were the only ones that contained no β-sheet structure. Peptide assembly upon dilution into PBSA could be highly sensitive to the balance between the rate of conversion to β-sheet-containing conformations (which would be a more important step for samples diluted from 100% DMSO than for other samples) and the rate of fibril initiation from the hypothesized β-sheet dimers. No fibrils would form until a sufficient concentration of β-sheet dimers built up. Once this happened, new dimers could be incorporated into the growing fibril or could self-assemble to initiate additional fibrils. Which is more likely to happen depends in a highly nonlinear way on the rate of production of dimers, the rate of association of dimers into multimers,

and the rate of addition of dimers to the growing fibril. Small differences in initial conditions could potentially lead to large differences in the final fibril length.

When diluted from ACN/TFA, the peptide aggregated quickly into extremely long fibrils. In ACN/TFA, the peptide retained the same β-sheet content as a solution of fibrils at physiological pH. This solvent is likely to disrupt hydrophobically and electrostatically driven association, which could therefore prevent extensive self-assembly of β-sheet conformers into the hypothesized multimers for fibril initiation. It is possible that more extensive hydrogen-bonded single β-sheets are present in this solvent than in any of the other stock solutions. In contrast, a significant fraction of the peptide was present as relatively short, amyloid fibrils in 10% DMSO, but these fibrils did not increase in length upon dilution into PBSA as quickly as the fibrils from the ACN/TFA solution. The difference between the two samples could be explained by postulating that the difference in starting condition leads to fewer, longer fibrils in the case of ACN/TFA stock solvent and more numerous, shorter fibrils for the 10% DMSO stock solvent, possibly resulting from the competition between fibril initiation versus fibril elongation.

It is interesting to note that $D_{z,m}^{-1}$ for β(1–28) in PBSA, when predissolved in 0.1% TFA, is significantly greater than for β(1–39) (Shen et al., 1993). Thus, fibrils formed from β(1–28) are significantly longer than β(1–39) fibrils, but β(1–28) has a larger fraction of peptide in nonfibrillar form and is less neurotoxic (Yankner et al., 1990). This suggests that perhaps self-assembly of β(1–28) is limited by fibril initiation, not by fibril elongation, to a greater extent than β(1–39).

We thus envision a model of self-assembly of Aβ that incorporates the following steps: (1) conversion of monomer to β-sheet peptide, possibly dimeric and possibly corresponding to the β-crystallites detected by x-ray diffraction (Inouye et al., 1993); (2) fibril initiation by association of dimers into multimers, perhaps similar to the pentameric or hexameric structures seen on cross section in some micrographs (Fraser et al., 1991b); (3) fibril growth by addition of β-sheet dimer to fibrils; (4) continued fibril elongation by end-to-end association of shorter fibrils; (5) entanglement or loose association of fibrils into clusters; and (6) precipitation when fibrils get sufficiently long and sufficiently numerous. From analysis of our data, we propose that the rate of dissociation of the hypothesized β-sheet dimer to the non-β-sheet monomer is slow relative to the rate of fibril initiation by self-assembly of dimers into higher order multimers. We further postulate that fibril initiation is slower and has a higher reaction order than fibril growth by addition of dimer. Any multimeric (fibril initiator) species that formed slowly but reacted rapidly would be present in virtually undetectable concentration. This model could account for the observation that addition (seeding) of preformed fibrils induces peptide aggregation (Jarrett et al., 1993; Snyder et al., 1994). The number, density, and length of fibrils depends on the balance between initial β-sheet

peptide content and rates of conversion of monomer to β-sheet dimer, fibril initiation, and fibril elongation. It is unlikely that a simple characterization of aggregation such as ThT fluorescence or centrifugation suffices to describe the complex peptide self-assembly process, to evaluate the role of self-assembly in neurotoxicity, or to determine the efficacy of potential inhibitors of Aβ assembly.

REFERENCES

Abe, E., F. Casamenti, L. Giovannelli, C. Scali, and G. Pepeu. 1994. Administration of amyloid beta-peptides into the medial septum of rats decreases acetylcholine release from hippocampus in vivo. *Brain Res.* 636:162–4.

Barrow, C. J., A. Yasuda, P. T. M. Kenny, and M. G. Zagorski. 1992. Solution conformations and aggregational properties of synthetic amyloid β-peptides of Alzheimer's disease. *J. Mol. Biol.* 225:1075–1093.

Burchard, W. 1977. Particle scattering factors of some branched polymers. *Macromolecules.* 10:919–927.

Burchard, W., and M. Muller. 1980. Statistics of branched polymers composed of rod substructures: a model for fibrin before clot formation. *Int. J. Biol. Macromol.* 2:225–234.

Burchard, W., M. Schmidt, and W. H. Stockmayer. 1980. Information of polydispersity and branching from combined quasi-elastic and integrated scattering. *Macromolecules.* 13:1265–1272.

Busciglio, J., A. Lorenzo, and A. B. Yankner. 1992. Methodological variables in the assessment of beta amyloid neurotoxicity. *Neurobiol. Aging.* 13:609–612.

Busciglio, J., J. Yeh, and B. A. Yankner. 1993. β-amyloid neurotoxicity in human cortical culture is not mediated by excitotoxins. *J. Neurochem.* 61:1565–1568.

Cohn, E. F., and J. T. Edsall. 1943. Proteins, Amino Acids and Peptides. Reinhold Publishing Co., New York. 372 pp.

Drogemeier, J., H. Hinssen, and W. Eimer. 1994. Flexibility of F-actin in aqueous solution: a study on filaments of different average length. *Macromolecules.* 27:87–95.

Fraser, P. E., L. K. Duffy, M. B. O'Malley, J. Nguyen, H. Inouye, and D. A. Kirschner. 1991a. Morphology and antibody recognition of synthetic β-amyloid peptides. *J. Neurosci. Res.* 28:474–485.

Fraser, P. E., D. R. McLachlan, W. K. Surewicz, C. A. Mizzen, A. D. Snow, J. T. Nguyen, and D. A. Kirschner. 1994. Conformation and fibrillogenesis of Alzheimer Aβ peptides with selected substitution of charged residues. *J. Mol. Biol.* 244:64–73.

Fraser, P. E., J. T. Nguyen, W. K. Surewicz, and D. A. Kirschner. 1991b. pH-dependent structural transitions of Alzheimer amyloid peptides. *Biophys. J.* 60:1190–1201.

Fraser, P. E., J. T. Nguyen, H. Inouye, W. K. Surewicz, D. J. Selkoe, M. B. Podlisny, and D. A. Kirschner. 1992. Fibril formation by primate, rodent, and Dutch-hemorrhagic analogues of Alzheimer amyloid β-protein. *Biochemistry.* 31:10716–10723.

Games, D., D. Adams, R. Alessandrini, R. Barbour, P. Berthelette, C. Blackwell, T. Carr, J. Clemens, T. Donaldson, F. Gillespie, T. Guido, S. Hagopian, K. Johnson-Wood, K. Khan, M. Lee, P. Leibowitz, I. Lieberburg, S. Little, E. Masliah, L. McConlogue, M. Montoya-Zavala, L. Mucke, L. Paganini, E. Penniman, M. Power, D. Schenk, P. Seubert, B. Snyder, F. Soriano, H. Tan, H. Vitale, S. Wadsworth, B. Wolozin, and J. Zhao. 1995. Alzheimer-type neuropathology in transgenic mice overexpressing V717F β-amyloid precursor protein. *Nature.* 373:523–527.

Gamini, A., and M. Mandel. 1994. Physicochemical properties of aqueous xanthan solutions: static light scattering. *Biopolymers.* 34:783–797.

Good, T. A., and R. M. Murphy. 1995. Aggregation state-dependent binding of β-amyloid peptide to protein and lipid components of rat cortical homogenates. *Biochem. Biophys. Res. Commun.* 207:209–215.

Hilbich, C., B. Kisters-Woike, J. Reed, C. L. Masters, and K. Beyreuther. 1991. Aggregation and secondary structure of synthetic amyloid βA4 peptides of Alzheimer's disease. *J. Mol. Biol.* 218:149–163.

Huber, K., and W. Burchard. 1989. Scattering behavior of wormlike star macromolecules. *Macromolecules.* 22:3332–3336.

Inouye, H., Fraser, P. E., and D. A. Kirschner. 1993. Structure of β-crystallite assemblies formed by Alzheimer β-amyloid protein analogues: analysis by x-ray diffraction. *Biophys. J.* 64:502–519.

Jackson, M., and H. H. Mantsch. 1991. Beware of proteins in DMSO. *Biochim. Biophys. Acta.* 1078:231–235.

Jarrett, J. T., E. P. Berger, P. T. Lansbury, Jr. 1993. The carboxy terminus of the β amyloid protein is critical for the seeding of amyloid formation: implications for the pathogenesis of Alzheimer's Disease. *Biochemistry.* 32:4693–4697.

Kang, J., H.-G. Lemaire, A. Unterbeck, J. M. Salbaum, C. L. Masters, K.-H. Grzeschik, G. Multhaup, K. Beyreuther, and B. Muller-Hill. 1987. The precursor of Alzheimer's disease amyloid A4 protein resembles a cell-surface receptor. *Nature.* 325:733–736.

Kirschner, D. A., H. Inouye, L. K. Duffy, A. Sinclair, M. Lind, and D. J. Selkoe. 1987. Synthetic peptide homologous to β protein from Alzheimer disease forms amyloid-like fibrils in vitro. *Proc. Natl. Acad. Sci. USA.* 84:6953–6957.

Koh, J.-Y., L. L. Yang, and C. W. Cotman. 1990. β-amyloid protein increases the vulnerability of cultured cortical neurons to excitotoxic damage. *Brain Res.* 533:315–320.

Koppel, D. E. 1972. Analysis of macromolecular polydispersity in intensity correlation spectroscopy: the method of cumulants. *J. Chem. Phys.* 57:4814–4820.

Kovacs, H., and A. Laaksonen. 1991. Molecular dynamics simulation and NMR study of water-acetonitrile mixtures. *J. Am. Chem. Soc.* 113: 5596–5605.

Koyama, R. 1973. Light scattering of stiff chain polymers. *J. Phys. Soc. Jpn.* 34:1029–1038.

Kuntz, I. D., Jr., and W. Kauzmann. 1974. Hydration of proteins and polypeptides. *Adv. Protein Chem.* 28:239–245.

LeVine, H., III. 1993. Thioflavin T interaction with synthetic Alzheimer's disease β-amyloid peptides: detection of amyloid aggregation in solution. *Protein Sci.* 2:404–410.

Loo, D. T., A. Copani, C. J. Pike, E. R. Whittemore, A. J. Walencewicz, and C. W. Cotman. 1993. Apoptosis is induced by β-amyloid in cultured central nervous system neurons. *Proc. Natl. Acad. Sci. USA.* 90: 7951–8055.

Luzar, A., and D. Chandler. 1993. Structure and hydrogen bond dynamics of water-dimethyl sulfoxide mixtures by computer simulations. *J. Chem. Phys.* 98:8160–8173.

Mant, C. T., and R. S. Hodges. 1992. Effects of HPLC solvents and hydrophobic matrices on denaturation of proteins. *In* High-Performance Liquid Chromatography of Peptides and Proteins: Separation, Analysis, and Conformation. C. T. Mant and R. S. Hodges, editors. CRC Press, Boca Raton, FL. 437–450.

Marcus, Y., and Y. Migron. 1991. Polarity, hydrogen bonding, and structure of mixtures of water and cyanomethane. *J. Phys. Chem.* 95: 400–406.

Masters, C. L., G. Simms, N. A. Weinman, G. Multhaup, B. L. McDonald, and K. Beyreuther. 1985. Amyloid plaque core proteins in Alzheimer disease and Down syndrome. *Proc. Natl. Acad. Sci. USA.* 82: 4245–4249.

Mattson, M. P., B. Cheng, D. Davis, K. Bryant, I. Lieberburg, R. E. Rydel. 1992. β-amyloid peptides destabilize calcium homeostasis and render human cortical neurons vulnerable to excitotoxicity. *J. Neurosci.* 12: 376–389.

Mattson, M. P., K. P. Tomaselli, and R. E. Rydel. 1993. Calcium-destabilizing and neurodegenerative effects of aggregated β-amyloid peptide are attenuated by basic FGF. *Brain Res.* 621:35–49.

Merz, P. A., H. M. Wisniewski, R. A. Somervill, S. A. Bobin, C. L. Masters, and K. Iqbal. 1981. Ultrastructural morphology of amyloid fibrils from neuritic and amyloid plaques. *Acta Neuropathol.* 60: 113–124.

Migron, Y., and Y. Marcus. 1991. Polarity and hydrogen-bonding ability of some binary aqueous-organic mixtures. *J. Chem. Soc. Faraday Trans.* 87:1339–1343.

Pike, C. J., D. Burdick, A. F. Walencewicz, C. G. Glabe, and C. W. Cotman. 1993. Neurodegeneration induced by β-amyloid peptides in vitro: the role of peptide assembly state. *J. Neurosci.* 13:1676–1687.

Pike, C. J., A. J. Walencewicz, C. G. Glabe, and C. W. Cotman. 1991. Aggregation-related toxicity of synthetic β-amyloid protein in hippocampal cultures. *Eur. J. Pharmacol.* 207:367–368.

Prelli, F., E. Castano, G. G. Glenner, and B. Frangione. 1988. Differences between vascular and plaque core amyloid in Alzheimer's disease. *J. Neurochem.* 51:648–651.

Schmidt, M., G. Paradossi, and W. Burchard. 1985. Remarks on the determination of chain stiffness from static scattering experiments. *Makromol. Chem.* 6:767–772.

Seery, T. A. P., M. Yassini, T. E. Hogen-Esch, and E. J. Amis. 1992. Static and dynamic light scattering characterization of solutions of hydrophobically associating fluorocarbon-containing polymers. *Macromolecules.* 25:4784–4791.

Shen, C.-L., M. C. Fitzgerald, and R. M. Murphy. 1994. Effect of acid predissolution on fibril size and fibril flexibility of synthetic β-amyloid peptide. *Biophys. J.* 67:1238–1246.

Shen, C.-L., G. L. Scott, F. Merchant, and R. M. Murphy. 1993. Light scattering analysis of fibril growth from the amino-terminal fragment β(1–28) of β-amyloid peptide. *Biophys. J.* 65:2383–2395.

Snyder, S. W., U. S. Ladror, W. S. Wade, G. T. Wang, L. W. Barrett, E. D. Matayoshi, H. J. Huffaker, G. A. Krafft, and T. F. Holzman. 1994. Amyloid-β aggregation: selective inhibition of aggregation in mixtures of amyloid with different chain lengths. *Biophys. J.* 67:1216–1228.

Soreghan, B., Kosmoski, J., and C. Glabe. 1994. Surfactant properties of Alzheimer's Aβ peptides and the mechanism of amyloid aggregation. *J. Biol. Chem.* 269:28551–28554.

Sorimachi, K., and D. J. Craik. 1994. Structure determination of extracellular fragments of amyloid proteins involved in Alzheimer's disease and Dutch-type hereditary cerebral haemorrhage with amyloidosis. *Eur. J. Biochem.* 219:237–251.

Stewart, W. E., and J. P. Sorensen. 1981. Bayesian estimation of common parameters from multiresponse data with missing observations. *Technometrics.* 23:131–141.

Sweeney, P. J., J. G. Darker, W. A. Neville, J. Humphries, and P. Camilleri. 1993. Electrophoretic techniques for the analysis of synthetic amyloid β-A4-related peptides. *Anal. Biochem.* 212:179–184.

Ueda, K., Y. Fukui, and H. Kageyama. 1994. Amyloid beta protein-induced neuronal cell death: neurotoxic properties of aggregated amyloid beta protein. *Brain Res.* 639:240–244.

Whitson, J. S., M. P. Mims, W. J. Strittmatter, T. Yamaki, J. D. Morrisett, and S. H. Appel. 1994. Attenuation of the neurotoxic effect of Aβ amyloid peptide by apolipoprotein E. *Biochem. Biophy. Res. Commun.* 199:163–170.

Wong, C. W., V. Quaranta, and G. G. Glenner. 1985. Neuritic plaques and cerebrovascular amyloid in Alzheimer disease are antigenically related. *Proc. Natl. Acad. Sci. USA.* 82:8729–8732.

Yamakawa, H., and M. Fujii. 1973. Translational friction coefficient of wormlike chains. *Macromolecules.* 6:407–415.

Yankner, B. A., L. K. Duffy, and D. A. Kirschner. 1990. Neurotrophic and neurotoxic effects of amyloid β-protein: reversal by tachykinin neuropeptides. *Science.* 250:279–282.